A&A 398, 967–973 (2003)
DOI: 10.1051/0004-6361:20021694

Astronomy & Astrophysics

XMM–Newton observations of the Seyfert 1 galaxy ESO 141–G55

P. Gondoin, A. Orr, and D. Lumb

Research and Scientific Support Department, European Space Agency – Postbus 299, 2200 AG Noordwijk, The Netherlands

Received 10 July 2002 / Accepted 13 November 2002

Abstract. We report on an observation of the Seyfert 1 galaxy ESO 141–G55 performed in October 2001 with the EPIC MOS cameras and Reflection Grating Spectrometers (RGS) on board the *XMM–Newton* observatory. We find the hard (3–10 keV) continuum slope, including reflection, to be somewhat flatter ($\Gamma = 1.72 \pm 0.06$) than that of a typical broad-line Seyfert 1 galaxy. The spectrum shows a weak emission line at 6.45 ± 0.04 keV with a measured equivalent width of ≈40 eV. A broad spectral feature is observed around 7 keV that can be fitted by an absorption edge at 7.6 ± 0.1 keV. The extrapolation of the primary power law continuum to energies lower than 2 keV indicates the presence of a soft excess component contributing to 45 ± 3% of the overall flux in the 0.3−2.0 keV energy range. This soft-excess cannot be explained solely by enhanced reflection from a highly ionized disk.

Key words. galaxies: individual: ESO 141–G55 – galaxies: nuclei – galaxies: Seyfert

1. Introduction

ESO 141–G55 is a bright but not well studied galaxy at a redshift $z = 0.0371 \pm 0.0003$ (de Vaucouleurs et al. 1991). It was first identified as a Seyfert 1 by Elvis et al. (1978) from the X-ray *Ariel* 5 survey list of Cooke et al. (1978) and confirmed as such by Ward et al. (1978). Optical and UV variability has been reported by Chapman et al. (1985), Morris & Wardt (1988), Winkler et al. (1992) and Winkler (1992). Using data from the *IUE* archives, Koratkar & Gaskell (1991) obtained lags of ≈30 and ≈90 lt-days between the variations of the UV continuum and the response of the Lyα and C IV λ1549 lines respectively. There are also evidence of variability in the X-ray bands. *EXOSAT* observations (Turner & Pounds 1989) showed a flat 0.1–10 keV spectrum with $\Gamma = 1.52\ ^{+0.03}_{-0.06}$ while the spectrum obtained with the *Einstein* Solid State Spectrometer and Monitor Proportional Counter (Turner et al. 1991) was much steeper ($\Gamma = 1.97 \pm 0.15$). The *ROSAT* best-fit PSPC spectrum (Turner et al. 1993) in the soft 0.1–2.4 keV band is even steeper ($\Gamma = 2.39 \pm 0.09$) and suggests the presence of a soft excess. Recent *BeppoSAX* data (Petrucci et al. 2001) did not confirm the presence of such component nor show evidence of warm absorber features.

The presence of a soft X-ray excess has been established in a large fraction of Seyfert galaxies (Turner & Pounds 1989; Walter & Fink 1993). A significant fraction of type 1 active galactic nuclei (Reynolds 1997) also show K-shells absorption edges of warm oxygen (O VII and O VIII) characteristic of optically thin, photoionized material along the line of sight to the central engine, the so-called warm absorber. The limitation in throughput, bandwidth or resolution of previous instruments and the presence of several components in the X-ray spectrum make the origin of the soft excess and warm absorber still unclear. A good determination of the shape of the intrinsic power law which should take into account the presence of a reflection component at high energies is particularly important for measuring the soft X-ray excess. In this respect, the present study of ESO 141-G55 benefits from the wide spectral band coverage and the large collecting area of the *XMM–Newton* space observatory.

In this paper, we report the analysis results of *XMM–Newton* observations of ESO 141-G55 performed in October 2001. Section 2 details the observations and data reduction procedures. Section 3 presents the integrated flux measurements and their temporal behaviour during the observations. The spectral analysis is reported in Sect. 4. The analysis results are discussed in Sect. 5.

2. Observations and data reduction

ESO 141-G55 was observed by the *XMM–Newton* space observatory (Jansen et al. 2001) between 2001 October 9 21:21:55 (UT) and 2001 October 10 13:23:00 (UT) for usable exposure times of 57.0 ksec (EPIC MOS 1 and MOS 2 cameras) and 57.6 ksec (RGS 1 and RGS 2 reflection grating spectrometers). *XMM–Newton* uses three grazing incidence telescopes which provide an effective area >4000 cm^2 at 2 keV and 1600 cm^2 at 8 keV (Gondoin et al. 2000). Three EPIC CCD cameras (Strüder et al. 2001; Turner et al. 2001) at the prime focus of the telescopes provide imaging in a 30′ field of view and broadband spectroscopy with a resolving power of between 5 and 60 in the energy range 0.3 to 10 keV. Two identical RGS

Send offprint requests to: P. Gondoin,
e-mail: pgondoin@rssd.esa.int

reflection grating spectrometers behind two of the X-ray telescopes allow high resolution ($E/\Delta E$ = 100 to 500) measurements in the soft X-ray range (6 to 38 Å or 0.3 to 2.1 keV) with a maximum effective area of about 140 cm^2 at 15 Å (den Herder et al. 2001).

The observations of ESO 141-G55 were conducted with the EPIC MOS cameras operating in full frame mode. RGS spectra were recorded simultaneously. "Medium" thickness aluminum filters were used in front of all CCD cameras to reject visible light. The EPIC pn camera was temporarily disabled during the observation. The large count rate of the target produced pile-up effects in the core of the telescope point spread functions registered by the EPIC MOS cameras. In order to reject these ambiguous events, the source spectra in the EPIC MOS cameras were built from photons detected within an annulus of radius included between 11″ and 86″ from the target boresight. The background was estimated on the same CCD chips within circular windows of 87″ radius which were offset by about 4′ from the source centroid position. Background rates were found to be extremely low during the first 40 ksec of the observation with a slight increase during the last 15 ksec. The Pulse-Invariant (PI) spectra were rebinned such that each resultant channel had at least 25 counts per bin in the MOS spectra. χ^2 minimization was used for the spectral fitting. All such fits were performed using the XSPEC package (v11). The EPIC response matrices were generated using the SAS tasks "rmfgen" and "arfgen" taking into account the annular shape of the source extraction windows. The RGS response matrices were generated by the SAS task "rgsrmfgen".

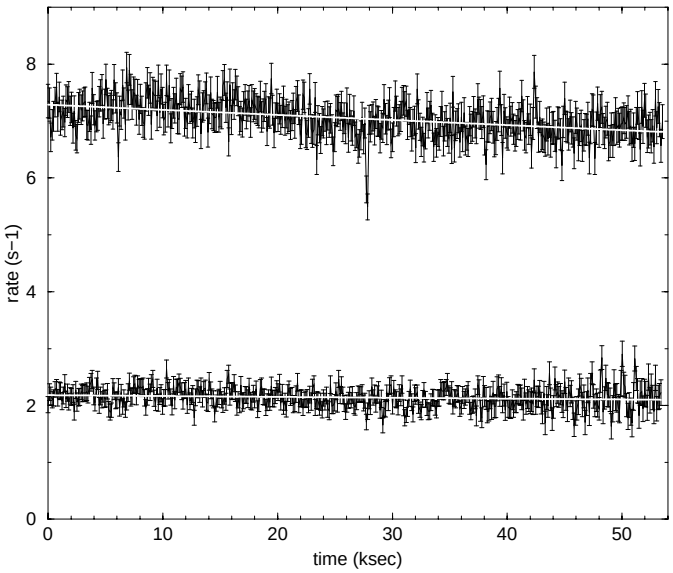

Fig. 1. Light curves of ESO 141-G55 obtained with the EPIC MOS cameras in the 0.3−2 keV (upper curve) and in the 2−10 keV (lower curve) energy bands. The noise rates have been subtracted. The events are binned into 120 s time intervals. The white lines are linear regressions to the light curves.

3. Integrated flux and temporal behaviour

The spectral analysis of the ESO 141-G55 *XMM–Newton* data (see Sect. 4) yields flux measurements in the low (0.3−2 keV) and high (2−10 keV) energy bands of $F_{\rm LE} = 2.24 \pm 0.05 \times 10^{-11}$ erg cm^{-2} s^{-1} and $F_{\rm HE} = 2.65 \pm 0.11 \times 10^{-11}$ erg cm^{-2} s^{-1}, respectively. After correction of the galactic absorption by hydrogen column density ($N_{\rm H} = 5.5 \times 10^{20}$ cm^{-2}), these correspond to luminosities of $L_{\rm LE} = 6.9 \times 10^{43}$ erg s^{-1} and $L_{\rm HE} = 8.1 \times 10^{43}$ ergs s^{-1} for $z = 0.0371$ and $H_0 = 75$ km s^{-1} Mpc^{-1}. The derived flux in the low energy band is comparable with the value derived in the 0.1–2 keV band from a *ROSAT* observation of ESO 141–G55 performed in 1991, 2.4×10^{-11} erg cm^{-2} s^{-1} (Turner et al. 1993). A linear regression to the light curves indicates a slight decrease of the source flux in the low and high energy bands (see Fig. 1). Over the 54 ksec observation period, the EPIC MOS count rates decreased by 6.8 ± 0.7% and 3.8 ± 1.4% in the 0.3−2 keV and 2−10 keV spectral band, respectively.

4. Spectral analysis

4.1. Phenomenological model of the high energy continuum and Fe K spectral features

In order to parametrize the high energy spectrum of ESO 141–G55, we first consider a single power-law model. A statistically acceptable fit to the 3–10 keV spectral band excluding the 4.5–8.0 keV iron K-shell region of the spectrum is obtained with a photon index $\Gamma = 1.72$. The best fit parameters are given in Table 1 (see Model A). Comparison of the data with the model shows an excess emission at 6.4 keV in the observed reference frame (see Fig. 2). Hence, we fitted the EPIC data in the 3–10 keV energy range by a phenomenological model consisting of an absorbed power law continuum and a Gaussian emission line. The best fit model to the EPIC $p-n$ data points to the existence of an iron Kα fluorescence line at 6.46 ± 0.03 keV. The best fit Gaussian model to the line (see Table 1, MODEL B) indicates an equivalent width $EW = 49 \pm 35$ eV. Since an emission line in Seyfert 1 galaxies is often associated with an absorption edge (e.g. Gondoin 2001a,b), we added an edge model to the redshifted Gaussian component. An absorption edge ($\tau = 0.33 \pm 0.09$) is detected at 7.6 ± 0.1 keV (see Table 1, MODEL C). The improvement in χ^2 fit statistics ($\Delta\chi^2/\Delta\nu = 8.5$ for 583 degrees of freedom) is significant at >99.9% confidence using the F-statistic. However, with so many degrees of freedom and so good a reduced χ^2, the presence of the edge shall be considered as probable rather than certain.

The iron Kα fluorescence line consists of two components Kα_1 and Kα_2 at 6.404 keV and 6.391 keV respectively for Fe I with a branching ratio of 2:1 (Bambynek et al. 1972). The natural width of the lines ($\Delta E \approx 3.5$ eV) and any broadening due to thermal motions of the emitting atoms (ΔE(eV) $\approx 0.4\ (T/10^6)^{1/2}$) are negligible compared to the energy resolution (155 eV FWHM) of the EPIC camera. The mean Fe Kα fluorescent line energy is an increasing function of ionization state. It rises slowly from 6.40 keV with Fe I to 6.45 keV in Fe XVII (neon-like) and then increases steeply with the escalating number of vacancies in the L-shell to 6.67 keV in Fe XXV and 6.9 keV in Fe XXVI (House 1969;

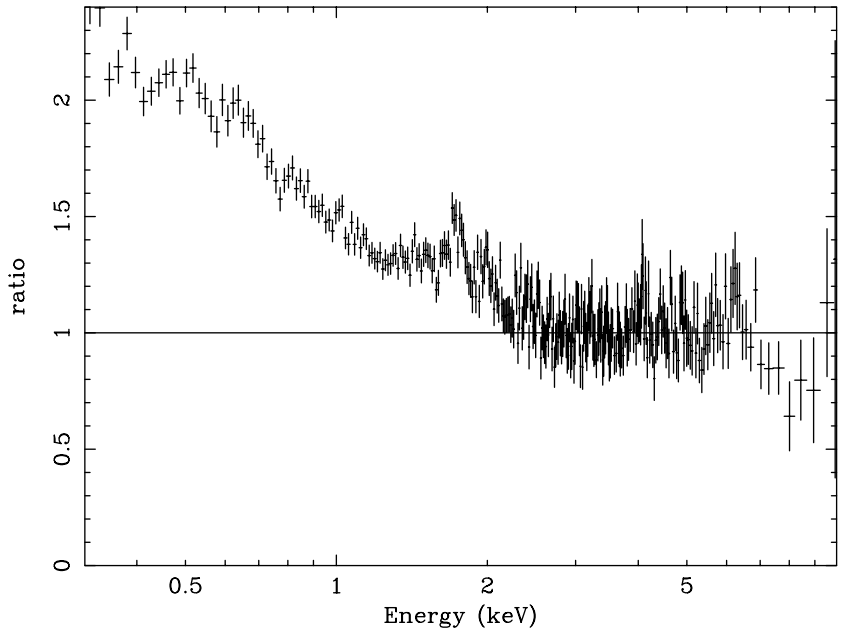

Fig. 2. Ratio between the EPIC MOS data and a best fit power law model to the 3–10 keV spectral band excluding the 4.5–8.0 keV iron K-shell region of the spectrum. The ratio shows a soft excess emission below 2 keV, a narrow emission feature around 6.5 keV and a broad trough above 7. Parameter ranges are given at a 90% confidence level.

Table 1. Phenomenological models of the ESO 141–G55 EPIC MOS spectra in the 3–10 keV spectral band. Spectral fitting with model A does not include the 4.5–7 keV energy range. For comparison, spectral fitting with model A including the 4.5–7 keV energy range gives a χ^2 of 608 for 588 degrees of freedom.

Component	Parameters	MODEL A	MODEL B	MODEL C
WABS	$N_{H,0}^{\rm gal}$ (cm^{-2})	5.5×10^{20}	5.5×10^{20}	5.5×10^{20}
ZPOWERLW	Γ	1.72 ± 0.06	1.76 ± 0.03	1.71 ± 0.03
ZGAUSS	E (keV)		6.46 ± 0.03	6.45 ± 0.03
	EW (eV)		44 ± 30	35 ± 23
ZEDGE	E (keV)			7.58 ± 0.09
	τ			0.33 ± 0.09
	χ^2_ν	242/250 d.o.f.= 0.97	595/585 d.o.f. = 1.02	578/583 d.o.f. = 0.99

Makishima 1986). Hence, the measured energy position of the Fe K line of ESO 141–G55 at 6.45 ± 0.03 keV indicates that iron is in a range of low states of ionization states, say ≤Fe XVII.

The energy of the Fe absorption edge is also a function of the ionization state of the Fe element. Aside from any blurring effect by the detectors spectral response, the iron K edge is not expected to be sharp due to electron scattering and by the presence of the iron Kβ line. Hence, the exact measurement of its position is difficult. In the case of Fe I, the K-shell absorption edge is at an energy $E_{\rm K}$ = 7.1 keV, rising to 7.8 keV for Fe XVIII, and 9.3 keV for Fe XXVI (Morita & Fujita 1983). The measured energy of the Fe K absorption edge of ESO 141–G55 at 7.6 ± 0.1 is consistent with the Fe Kα line position and indicates the presence of material where iron is in a range of low ionization states, up to say Fe XVII.

An alternative hypothesis not to be excluded is the existence of a broad underlying Fe Kα component which would amplify the absorption around 7.6 keV that we interpretate as an edge. If the red wing of this broad Kα component were present but not accounted for in the continuum fitting, it could tend to make the continuum between 4 and 6 keV appear flatter. In order to test this hypothesis, we fitted the 3–10 keV spectrum of NGC 3227 with a power law, a narrow Gaussian emission component and a broad accretion disk profile described by a DISKLINE (Fabian et al. 1989) or by a LAOR (Laor 1991) model. The DISKLINE model was used with a $(1-(6/R)^{1/2})/R^3$ emissivity law. The disk inner radius was fixed to $R_{\rm min} = 6.0 \times GM/c^2$ while the disk outer radius and inclination were left free to vary. The LAOR model was tested with two values $\beta = 2$ and 3 for a power law dependence, $R^{-\beta}$, of the emissivity. The disk inclination in the LAOR model was fixed to 30°. The POWERLW + DISKLINE or LAOR model provide a good fit to the data (χ^2_ν = 1.02; see Table 2). The slope index of the power law spectrum ($\Gamma = 1.79 \pm 0.04$) is steeper than the one derived using an absorption edge model. The position of the broad underlying Fe K component is poorly constrained by the LAOR models. Comparing Table 2 with model B of Table 1, no statistical improvement is found. Hence, the results of the fit obtained with relativistic line models indicate that the presence of a broad underlying Fe K component is not required to explain the high energy spectrum of ESO 141–G55.

Table 2. Best fit parameters to the EPIC Fe K spectral feature in the 3–10 keV band assuming a narrow Gaussian line and a broad emission component from a relativistic accretion disc. The relativistic line profile is described either by the DISKLINE model or by the LAOR model with a power law emissivity ($R^{-\beta}$).

Model parameters	LAOR(β = 2)	LAOR(β = 3)	DISKLINE
Line energy (keV)	6.55 ± 0.93	6.55 ± 1.2	6.4 ± 0.6
Line equivalent width (eV)	110 ± 70	98 ± 90	33
Inner radius (units of GM/c^2)	0–5.5	2.2 ± 1.9	6.0 (frozen)
Outer radius (units of GM/c^2)	6.3 ± 2.1	6.3 ± 3.4	7.4 ± 3.4
Disk inclination (°)	30 (frozen)	30 (frozen)	30.5 ± 7.4
χ^2_ν	593/582 d.o.f. = 1.02	592/582 d.o.f. = 1.02	591/582 d.o.f. = 1.02

4.2. Analysis of the soft energy range

In order to fully characterize the continuum emission of ESO 141–G55, we extended the analysis of EPIC data to the 0.3–10 keV energy range. Comparisons of the spectra with the best fit power law model established above 3 keV show large residuals at soft energies (see Fig. 2). This led us to add a soft excess component to the power law and absorption edge model (see Table 1, MODEL C). We tested a blackbody, a Bremsstrahlung and a second power law component. The three component models were combined with neutral galactic absorption using the cross-sections of Morrison & McCammon (1983) assuming galactic absorption with solar abundance and $N_{\rm H} = 5.5 \times 10^{20}$ cm^{-2} (Turner et al. 1993). The power law and the blackbody models give an unacceptable fit to the soft excess-emission, with a reduced χ^2 of respectively 1.28 and 1.40. The redshifted power law + thermal Bremsstrahlung model provides a good description of the spectrum ($\chi^2 = 1.13$). We find a Bremsstrahlung temperature $kT = 0.44 \pm 0.08$ keV for a power law index frozen to $\Gamma = 1.71$ (see Table 3). The Bremsstrahlung model for this temperature regime is regarded as a parametrization of the source continuum emission at soft energies and not as a physically consistent model. The integrated Bremstrahlung emission over the 0.3 to 2 keV spectral band measures the soft excess emission above the power law. It represents 45 ± 3% of the intrinsic source flux in that band after correction for Galactic absorption and less than 1% of the intrinsic source flux above 2 keV.

Evidence for ionized accretion discs have been found in particular in narrow line Seyfert 1 galaxies (TON S 180: Comastri et al. 1998; Turner et al. 1998; Ark 564: Vaughan et al. 1999; Gondoin et al. 2002). These conclusions are based on either the energy centroid of the observed Fe Kα line or on spectral fits using the PEXRIV ionized disc model of Magdziarz & Zdziarski (1995). Ionized reflection has observable effects over the whole X-ray continuum, so tighter constraints on the ionization state can be obtained by fitting the ionized disc model over the entire observed energy range. The PEXRIV model alone does not gives an acceptable fit to the data with a reduced χ^2 of 1.33 and an unphysically high reflection fraction. Hence, we combined this model with a Bremstrahlung soft excess component. The best fit parameters of the combined model are listed in Table 3. The PEXRIV model was used with a disk temperature fixed at 1.2×10^5 K, a disk inclination angle fixed at 30° and a disk abundance set to the solar value. The power law cut-off energy was set at 100 keV. One major variable in reflection models is the ionisation parameter ξ of the slab ($\xi = 4\pi \times F/n$) where F is the incident flux (ergs s^{-1} cm^{-2}) and n is the hydrogen number density of slab (cm^{-3}). The PEXRIV model gives a ionization parameter $\xi \leq 270$ ergs cm s^{-1} corresponding to a reflection of the primary power law component by low or moderately ionized material. The contribution of the Bremstrahlung component is not reduced compared to the model without reflection. Since the iron spectral feature could include a broad underlying Fe Kα component, we tested the PEXRIV reflection model from ionized material in combination with the emission line from an accretion disk around a black hole using the LAOR model. In PEXRIV, the relativistic smearing is not applied to the reflection continuum. Hence, we also tested the REFSCH+DISKLINE model. In this model, an exponentially cut-off power-law spectrum reflected from an ionized relativistic accretion disk (Magdziarz & Zdziarski 1995) is convolved with a relativistic disk line profile. The PEXRIV+LAOR model and the REFSCH+DISKLINE model do not give acceptable fits to the data even when they are combined with a Bremstrahlung soft excess component.

As shown by Ross et al. (1999), the PEXRIV model is inaccurate as the disc becomes highly ionized. Therefore, we fitted the EPIC spectra with the constant density ionised disc models of Ross & Fabian (1993; see also Ballantyne et al. 2001). These models (hereafter called RF models) calculate the spectrum of an input power-law after reflection from an ionized slab. They include lines and edges from Fe, O, Si, Mg, and C and are valid over the energy range 1 eV–100 keV. A larger ionisation parameter, i.e. a more ionized gas, reduces the strength and width of the features in the reflected spectrum including the Fe Kα line and the various absorption edges (Matt et al. 1993, 1996). The computed reflection spectrum is multiplied by a factor R, where R is the reflection fraction, and then added to the illuminating spectrum to produce the model spectrum. Fits with the RF model alone did not provide acceptable results, with a reduced χ^2_ν of 1.37 for 942 degrees of freedom. Hence we also combined the RF model with a Bremstrahlung component. The combined model provides a fit to the data with a reduced χ^2_ν of 1.24 (see Table 3). A comparison of the best fit parameters with those obtained using the PEXRIV model shows that spectral fitting with the RF model leads to a higher ionization parameter, $\xi = 6400 \pm 1800$ erg cm s^{-1} (to be compared with $\xi < 1200$ for PEXRIV using a conversion factor $\xi_{\rm RF}/\xi_{\rm PEXRIV} = 4.4$). The temperature of the Bremstrahlung

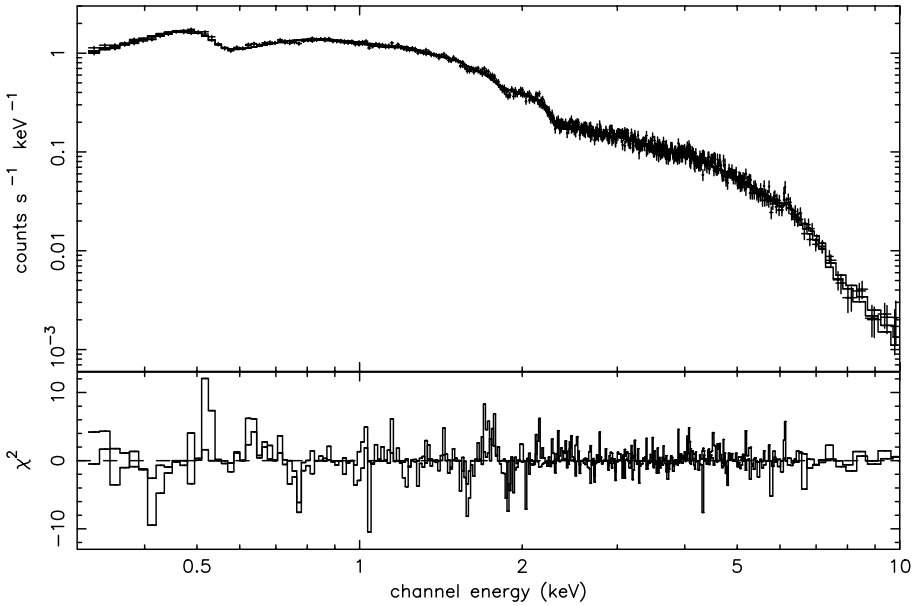

Fig. 3. EPIC MOS spectra of ESO 141–G55 compared with the best fit absorbed power law + Bremstrahlung model. The data and spectral fit are shown in the upper panel. The χ^2 contributions are plotted in the lower panel.

Table 3. Best fit parameters to EPIC MOS spectra with ionized reflection and soft excess Bremstrahlung emission models. The ionization parameter ξ is calculated either in the 0.01−100 keV band (RF model) or in the 5−20 keV band (PEXRIV model). A comparison between these models requires the multiplication of the ionization parameter by a conversion factor $\xi_{\rm RF}/\xi_{\rm PEXRIV}$ ≈4.1–4.7 for a power law spectrum with $1.66 < \Gamma < 1.78$. The fraction flux is the relative contribution of the Bremstrahlung component to the source flux in the 0.3 to 2 keV range corrected from galactic absorption.

Component	Parameters	POWER LAW (+ ZEDGE)	PEXRIV	RF
WABS	$N_{\rm H}$ (cm^{-2})	5.5×10^{20} (frozen)	5.5×10^{20} (frozen)	5.5×10^{20} (frozen)
	kT (keV)	0.44 ± 0.08	0.42 ± 0.02	0.36 ± 0.01
ZBREMSS	Redshift	0.0371 (frozen)	0.0371 (frozen)	0.0371 (frozen)
	Fraction flux	45 ± 3%	42 ± 1%	17 ± 1%
	Γ	1.71 (frozen)	1.72 ± 0.06	1.75 ± 0.01
	$E_{\rm c}$ (keV)		100 (frozen)	
Reflection	R		0.0–0.5	1.0 (frozen)
Model	Abundance		1.0 (frozen)	
	Inclination (°)		30.0 (frozen)	
	$T_{\rm disk}$ (K)		1.2×10^5 (frozen)	
	ξ (erg cm s^{-1})		0–270	6400 ± 2800
	χ^2_ν	1067/940 d.o.f. = 1.13	1168/939 d.o.f. = 1.24	1165/941 d.o.f. = 1.24

component, $kT = 0.36$ keV is lower than in the previous cases and its relative contribution to the overall spectrum is reduced by a factor of 2–3 compared with a simple power law model without reflection. Reflection of the primary power law component by highly ionized material with constant density can only account for about 60% of the observed soft excess emission.

The high spectral resolution of the RGS spectrometers on board *XMM–Newton* is well suited to disentangle emission line features from absorption edges and to detect the presence of an absorber or emitter in the 0.3 to 2.1 keV energy band. The RGS spectrum of ESO 141–G55 shows no strong features between 6 and 38 Å (0.3–2 keV) other than the absorption edge of neutral interstellar oxygen at 23.3 Å (see Fig. 4). In particular, no evidence is found for K−shells absorption edges at 0.74 keV (OVII) and 0.85 keV (OVIII) characteristic of the presence of ionized material along the line of sight. The spectral fit with the power law and reflection model combined with a Bremstrahlung component, as described in Table 3, gives an acceptable fit to the RGS data. However, the signal to noise ratio of the RGS data does not permit to place further constraints on the Bremstrahlung component. Acceptable spectral fit of the RGS data can also be obtained with a power law or a blackbody model.

5. Discussion

The power law X-ray emission of radio-quiet AGNs is likely the result of inverse Compton scattering of low-energy photons by relativistic electrons. Although the geometry of the region

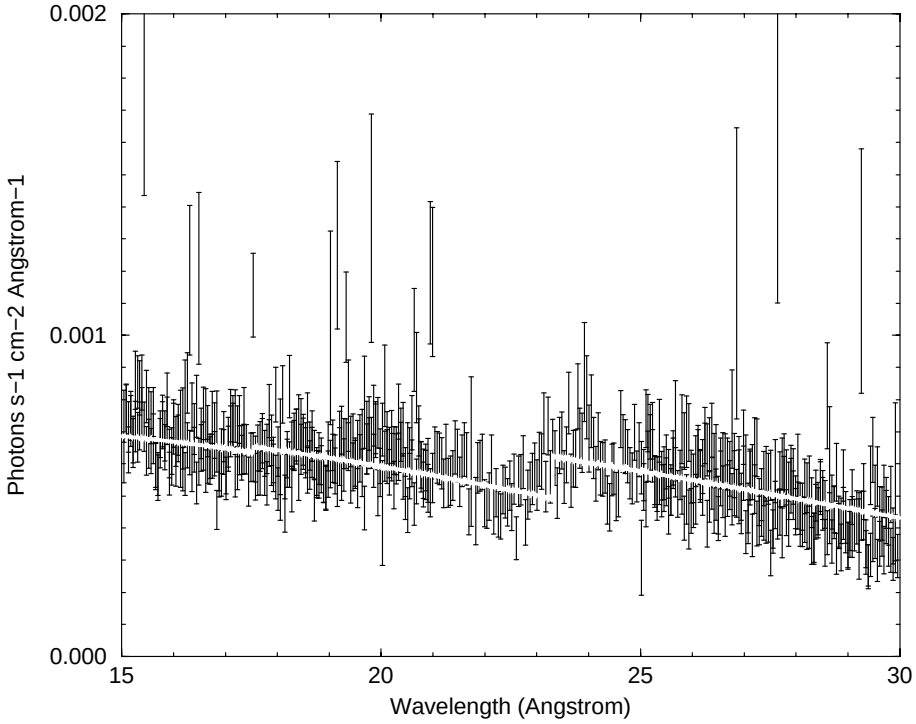

Fig. 4. The 15–30 Å RGS spectrum of ESO 141–G55. The continuous line represent the spectrum of an absorbed power law plus Bremstrahlung emission.

emitting the primary X-ray spectrum is unknown, the general consensus is that the power law component originates from an extended corona in the vicinity of an accretion disk (Haardt & Matt 1993). Within the context of such a model, the Fe K emission in the spectrum of ESO 141–G55 and its soft excess emission could be produced by Compton reflection of the primary continuum onto an accretion disk. Possible contribution to these reflection components may come from material within the accretion disk itself (Pounds et al. 1990) or from matter further out (Krolik et al. 1994; Ghisellini et al. 1994). Orbital motion deep in a relativistic gravitational potential seems to be the probable interpretation for Fe K lines profiles that have been observed to be several tens of thousands of km s^{-1} broad and significantly redshifted (Mushotzky et al. 1995; Tanaka et al. 1995; Page et al. 2001; Wilms et al. 2001; Gondoin et al. 2002). Many AGNs show narrow Fe K lines (Gondoin et al. 2001a,b; Reeves et al. 2001a; Yaqoob et al. 2001). Also, a unique iron K emission line profile with two distinct components has been recently reported on Mrk 205 (Reeves et al. 2001b). The spectral feature observed around 6.0 keV in ESO 141–G55 spectrum includes a narrow Fe K emission line at 6.43 keV ($EW \approx$ 40 eV) and a broad feature that can be fitted by an absorption edge at 7.6 keV. The energy position of the Fe K line at 6.45 ± 0.03 keV indicates that iron is in low states of ionization. The gas of the reflection slab could apparently remain essentially cool despite being exposed to an intense flux of X-rays. Such a result can be interpreted as an indication that the gas in the accretion disk is dense (Guilbert & Rees 1988; Ferland & Rees 1988). The detected absorption edge at 7.64 keV indicates that atoms in different states of ionization ranging from neutral to Fe XVII may contribute to the absorption.

Comparisons of the MOS spectra of ESO 141–G55 in the 0.3–10 keV range with the best fit power law model established above 3 keV show large residuals at soft energies. In the low energy domain below 2 keV, we did not find evidence for the presence of emission lines or absorption edges other than the edge produced by galactic neutral oxygen. Explanations for a spectral steepening in the soft X-ray band based on reflection by ionized media have been successfully applied to a few AGNs (Zycki et al. 1994; Piro et al. 1997). According to these scenarios, the inner region of the disk could be photo-ionized by X-rays emitted from the primary continuum source. Spectral fitting of the ESO 141–G55 spectra with the RF model points to an ionization parameter greater than 3×10^3 erg cm s^{-1} implying that the material responsible for the soft X-ray emission is highly ionized and reflective to soft X-rays, thus leading to further enhancement of the soft X-ray excess. About 60% of the soft excess can be accounted by this reflection model from ionized material with a constant density. The other 40% contribution can be parametrized by a Bremstrahlung model with a temperature $T = 0.36 \pm 0.1$ keV. For ionization parameters lower than 10^3 erg cm s^{-1}, detailed models of this reflected component typically include line emission from O VIII ($E = 0.65$ keV) and O VII ($E = 0.57$ keV), with an equivalent width depending on the ionization parameter. The absence of such emission features around 0.6 keV in the RGS spectra of ESO 141–G55 supports a scenario where the reflecting material is highly ionized.

Illumination of a disk by hard X-rays leads to the formation of a very hot, optically thin layer of material above the disk (Krolik et al. 1981). In the hot layer, Comptonization and bremstrahlung play the main roles, but closer to the cool, dense

disc, atomic absorption and emission become the major cooling processes. Reflection effects of the primary continuum can be largely enhanced below 1.5 keV owing to Bremsstrahlung emission by the hot surface layer and "inverse Compton" upscattering of even softer photons. Depending on the hardness of the primary spectrum, the ionization parameter and the disk density, the temperature of the illuminated surface is found to be extremely high ($T > 10^7$ K) for constant density disk models (Ross et al. 1999). It is worth noting that a somewhat lower temperature ($T \approx 4 \times 10^6$ K) is suggested by the Bremstrahlung component of the best fit models to the spectrum of ESO 141–G55. Recently, Nayakshin et al. (2000) presented ionized reflection models where hydrostatic equilibrium is solved along with the ionization and radiation structure. They found that, for $\Gamma < 2$, the equivalent width of the Fe features decreases monotonically with the magnitude of the illuminating flux while the energy centroid of the Fe K line remains at 6.4 keV. The best fit Gaussian profile model to the narrow Fe K emission component in ESO 141–G55 suggests a weak features ($EW < 58$ eV) at an energy corresponding to emission from iron in low states of ionization. The strength of this Fe K line component could be understood if the accretion disk develops an overionized hot skin produced by the strong hard X-ray illumination. However, attempt to verify this hypothesis by fitting the EPIC MOS spectra of ESO 141-G55 using the XION model of the reflected spectra of a photo-ionized accretion disk illuminated by an X-ray source (Nayakshin et al. 2000) did not provide an acceptable fit to the data. The strong soft component seems not due only to disk reprocessing. Ionized reflection is only one viable possibility among other processes. Thermal emission produced by the viscous heating of the disk could significantly contribute to the soft excess. In that case, the soft radiation from the disk itself may participate significantly to the photoionization of most ionic species, so that an ionization parameter defined in terms of the illuminating flux would no longer describe the state of the gas.

Acknowledgements. We thank our colleagues from the *XMM–Newton* Science Operation Center for their support in implementing the observations. We are grateful to the anonymous referee for providing helpful comments on the manuscript.

References

Ballantyne, D. R., Iwasawa, K., & Fabian, A. C. 2001, MNRAS, 323, 506
Bambynek, W., Craseman B., Fink, R. W., et al. 1972, Rev. Mod. Phys., 44, 716
Chapman, G. N. F., Geller, M. J., & Hichra, J. P. 1985, ApJ, 297, 151
Comastri, A., Fiore, F., Guainazzi, M., et al. 1998, A&A, 333, 31
Cooke, B. A., Ricketts, M. J., Maccacaro, T., et al. 1978, MNRAS, 182, 489
den Herder, J. W., Brinkman, A. C., Kahn, S. M., et al. 2001, A&A, 365, L7
de Vaucouleurs, G., de Vaucouleurs, A., Corwin, H. G., et al. 1991, Third Reference Catalogue of Bright Galaxies (New York: Springer)
Elvis, M., Maccacaro, T., Wilson, A. S., et al. 1978, MNRAS, 183, 129
Fabian, A. C., Rees, M. J., Stella, L., et al. 1989, MNRAS, 238, 729
Ferland, G. J., & Rees, M. J. 1988, ApJ, 332, 141
Ghisellini, G., Haardt, F., & Matt, G. 1994, MNRAS, 267, 743
Gondoin, P., Aschenbach, B., Erd, C., et al. 2000, SPIE Proc., 4140, 1
Gondoin, P., Lumb, D., Siddiqui, H., et al. 2001a, A&A, 373, 805
Gondoin, P., Barr, P., Lumb, D., et al. 2001b, A&A, 378, 806
Gondoin, P., Orr, A., Lumb, D., et al. 2002, A&A, 388, 74
Guilbert, P. W., & Rees, M. J. 1988, MNRAS, 233, 475
Haardt, F., & Matt, G. 1993, MNRAS, 261, 346
House, L. L. 1969, ApJS, 18, 21
Jansen, F., Lumb, D., Altieri, B., et al. 2001, A&A, 365, L1
Koratkar, A. P., & Gaskell, C. M. 1991, ApJ, 370, 61
Krolik, J. H., Mc Kee, C. F., & Tarter, C. B. 1981, ApJ, 249, 422
Krolik, J. H., Madau, P., & Zycki, P. 1994, ApJ, 420, L57
Laor, A. 1991, ApJ, 376, 90
Magdziarz, P., & Zdziarski, A. A. 1995, MNRAS, 273, 837
Makishima, K. 1986, in The Physics of Accretion onto Compact Objects, ed. K. O. Mason, M. G. Watson, & N. E. White (Springer Verlag, Berlin), 250
Morita, S., & Fujita, J. 1983, J. Phys. Soc. Japan, 52, 1957
Morris, S., & Ward, M. 1988, MNRAS, 230, 639
Morrison, T., & McCammon, D. 1983, ApJ, 270, 119
Mushotzky, R. F., Fabian, A. C., Iwasawa K., et al. 1995, MNRAS, 272, L9
Nayakshin, S., Kazanas, D., & Kallman, T. R. 2000, ApJ, 537, 833
Page, M. J., Mason, K. O., Carrera, F. J., et al. 2001, A&A, 365, L152
Petrucci, P. O., Haardt, F., Maraschi, L., et al. 2001, ApJ, 556, 716
Piro, L., Balucinska-Church, M., Fink, H., et al. 1997, A&A, 319, 74
Pounds, K. A., Nandra, K., Stewart, G. C., et al. 1990, Nature, 344, 132
Reeves, J. N., Turner, M. J. L., Bennie, P. J., et al. 2001a, A&A, 365, L116
Reeves, J. N., Turner, M. J. L., Pounds, K. A., et al. 2001b, A&A, 365, L134
Reynolds, C. S. 1997, MNRAS, 286, 513
Reynolds, C. S., & Begelman, M.C. 1997, ApJ, 488, 109
Ross, R. R., Fabian, A. C., & Brandt, W. N. 1996, MNRAS, 278, 1082
Strüder, L., Briel, U., Dennerl, K., et al. 2001, A&A, 365, L18
Tanaka, Y., Nandra, K., & Fabian, A. C. 1995, Nature, 375, 659
Turner, T. J., & Pounds, K. A. 1989, MNRAS, 240, 833
Turner, T. J., Weaver, K. A., Mushotzky, R. F., et al. 1991, ApJ, 381, 85
Turner, T. J., George, I. M., & Mushotzky, R. F. 1993, ApJ, 412, 72
Turner, T. J., George, I. M., & Nandra, K. 1998, ApJ, 508, 648
Turner, M. J. L. T., Abbey, A., Arnaud, M., et al. 2001, A&A, 365, L27
Vaughan, S., Pounds, K. A., Reeves, J., et al. 1999, MNRAS, 308, L34
Walter, R., & Fink, H. H. 1993, A&A, 274, 105
Ward, M., Wilson, A. S., Penston, M. V., et al. 1978, ApJ, 223, 788
Wilms, J., Reynolds, C. S., Begelman, M. C., et al. 2001, MNRAS, 328, L27
Winkler, H. 1992, MNRAS, 257, 677
Winkler, H., Glass, I. S., van Wyk, F., et al. 1992, MNRAS, 257, 659
Yaqoob, T., George, I. M., Nandra, K. et al. 2001, ApJ, 546, 759
Zycki, P. T., Krolik, J. H., Zdziarski, A. A., et al. 1994, ApJ, 437, 597